Human Molecular Genetics, 2016, Vol. 25, No. 10 2031–2044

doi: 10.1093/hmg/ddw077
Advance Access Publication Date: 2 March 2016
Original Article

ORIGINAL ARTICLE

ARL3 regulates trafficking of prenylated phototransduction proteins to the rod outer segment

Zachary C. Wright[1], Ratnesh K. Singh[1], Ryan Alpino[1], Andrew F.X. Goldberg[4], Maxim Sokolov[1,2,3] and Visvanathan Ramamurthy[1,2,3,*]

[1]Department of Ophthalmology, [2]Department of Biochemistry and [3]Center for Neuroscience, Robert C. Byrd Health Sciences Center, West Virginia University, Morgantown, WA 26506, USA and [4]Eye Research Institute, Oakland University, Rochester, MI 48309, USA

*To whom correspondence should be addressed at: West Virginia University Eye Institute, One Medical Drive, E-363, Morgantown, WV 26506-9193, USA. Tel: +1 3045986940; Fax: +1 3045986928; Email: ramamurthyv@wvumedicine.org

Abstract

The small GTPase, ADP-ribosylation factor-like 3 (ARL3), has been proposed to participate in the transport of proteins in photoreceptor cells. Moreover, it has been implicated in the pathogenesis associated with X-linked retinitis pigmentosa (XLRP) resulting from mutations in the ARL3 GTPase activating protein, retinitis pigmentosa 2 (RP2). To determine the importance of ARL3 in rod photoreceptor cells, we generated transgenic mice expressing a dominant active form of ARL3 (ARL3-Q71L) under a rod-specific promoter. ARL3-Q71L animals exhibited extensive rod cell death after post-natal day 30 (PN30) and degeneration was complete by PN70. Prior to the onset of cell death, rod photoresponse was significantly reduced along with a robust decrease in rod phosphodiesterase 6 (PDE6) and G-protein receptor kinase-1 (GRK1) levels. Furthermore, assembled phosphodiesterase-6 (PDE6) subunits, rod transducin and G-protein receptor kinase-1 (GRK1) accumulated on large punctate structures within the inner segment in ARL3-Q71L retina. Defective trafficking of prenylated proteins is likely due to sequestration of prenyl binding protein δ (PrBPδ) by ARL3-Q71L as we demonstrate a specific interaction between these proteins in the retina. Unexpectedly, our studies also revealed a novel role for ARL3 in the migration of photoreceptor nuclei. In conclusion, this study identifies ARL3 as a key player in prenylated protein trafficking in rod photoreceptor cells and establishes the potential role for ARL3 dysregulation in the pathogenesis of RP2-related forms of XLRP.

Introduction

Trafficking of proteins to the right destination is crucial for proper functioning of a cell. The significance of this process is exemplified by polarized photoreceptor cells in the retina. In photoreceptors, proteins are synthesized in the inner segment (IS) and are selectively transported to their site of action in the outer segment (OS). In addition, the high rate of protein turnover resulting from the renewal of the OS requires an efficient mode of protein movement between various compartments in photoreceptor cells. Defective trafficking is a known cause of blinding diseases such as retinitis pigmentosa in humans (1,2). Despite the importance of efficient trafficking of proteins in photoreceptor cells, the basic mechanism behind the regulation and polarized movement of OS proteins are poorly understood.

Small GTPases are molecular switches cycling between GTP-bound 'on' and GDP-bound 'off' states and are known regulators of vesicular trafficking, aiding in the movement of proteins and lipids between different cellular compartments. ARL3, a member of the ADP-ribosylation factor (ARF) family, is one such GTPase that is important for photoreceptor development. Absence of ARL3 in a mouse knockout leads to poor development of photoreceptor cell OS and rapid degeneration of photoreceptor neurons (3). However, little is known about the role of ARL3 *in vivo* (4). ARL3 was identified as an effector protein of retinitis pigmentosa

Received: December 11, 2015. **Revised:** February 1, 2016. **Accepted:** February 29, 2016

protein 2 (RP2). RP2 acts as a GTPase activating protein (GAP) thereby facilitating conversion of active ARL3–GTP to inactive ARL3-GDP, accelerating the intrinsic GTPase activity up to 90 000-fold (5). Defects in the RP2 gene result in an X-linked form of retinitis pigmentosa (XLRP), a very severe form of inherited blindness in males. Mutations in this gene account for ~7–18% of these XLRP cases (6). Disruption of the RP2 gene likely leads to dysregulation of its interacting protein ARL3, maintaining it in an active, GTP-bound state as it would rely solely on its slow intrinsic rate (k_{cat} of 0.007/min) (5,7,8). Additionally, ARL3 has been implicated in the transport of lipid-modified proteins through its association with the lipid-binding proteins, prenyl-binding protein δ (PrBPδ; also known as PDE6δ) and the PrBPδ homolog Unc119 (also known as HRG4) (9–11). PrBPδ has a lipid-binding pocket that is exposed in the 'open' conformation and inaccessible in the 'closed' conformation. Active ARL3-GTP (but not the inactive ARL3-GDP) binds to an allosteric site that induces the change of PrBPδ to the 'closed' confirmation thereby lowering affinity for the prenyl group on an effector protein. These *in vitro* data suggest that ARL3 acts as a release factor for prenylated cargo being carried by PrBPδ (10). Related studies have shown that loss of PrBPδ in mice lead to defective trafficking of prenylated proteins to rod and cone OSs (12). More recently, it has been shown that RP2 knockout mice exhibit slow progressive retinal degeneration (7,13) associated with mislocalization of prenylated phosphodiesterase 6 (PDE6) and G-protein receptor kinase 1 (GRK1) (7). This result has also been recapitulated in RP2 null zebrafish, which showed slow degeneration and mislocalization of prenylated proteins (14). Absence of RP2 likely leads to overactive ARL3 as the GAP activity is lost. We believe that ARL3 overactivity is the intermediary that causes the phenotype observed in RP2 mouse models and associated human disease.

The purpose of the present study is to gain insight into the role of ARL3 in rod photoreceptor cells. ARL3 dysregulation, that is constitutive activation via ARL3-Q71L transgenic expression, leads to disrupted trafficking of prenylated proteins, including PDE6, GRK1 and transducin. Additionally, we show that active ARL3-Q71L and not ARL3-WT interacts with PrBPδ *in vivo*.

Results

ARL3-Q71L dominant active mutant transgenic model generation

To determine the role for ARL3 in photoreceptor function, we generated a transgenic animal expressing dominant active mouse ARL3-Q71L in rod photoreceptor cells (Fig. 1A). A control transgenic line expressing tagged wild-type mouse ARL3 (ARL3-WT) was also generated. Expression of both wild-type and dominant active ARL3 are under the control of a rhodopsin promoter that drives the expression of transgenes as early as post-natal day 4 (PN4) in rod photoreceptor cells of the retina (15). Transgenic founders were crossed with 129/SV-E wild-type mice over at least two generations to ensure consistent transgene inheritance and expression prior to analysis. Transgenic negative littermates of ARL3-Q71L mice were used as control animals for comparison unless stated otherwise.

We generated an affinity purified rabbit antibody against mouse ARL3. This antibody specifically recognized mouse ARL3 expressed in Human Embryonic Kidney (HEK293) cells (compare lanes 1 versus 2 in Fig. 1B). Immunoblotting using the custom made antibody comparing the tagged ARL3-Q71L band (~26 kDa) to the endogenous ARL3 band at ~23 kDa (Fig. 1B; $P < 0.001$) revealed 2.5-fold overexpression of mutant Q71L over endogenous ARL3 levels. Additionally, an anti-HA antibody was used to confirm the identity of the tagged ARL3-Q71L [Fig. 1B (green)]. ARL3-Q71L expression was also confirmed by indirect immunofluorescence with anti-ARL3 antibody and anti-HA antibody (Fig. 1C). ARL3-Q71L was found throughout rod photoreceptor cells from the synapse to the OS similar to endogenous ARL3 localization in transgenic negative and transgenic ARL-WT samples (Fig. 1C and Supplementary Material, Fig. S1). Because previous study utilizing immunofluorescence microscopy reported ARL3 to be primarily located in the photoreceptor's connecting cilium (16), we investigated the distribution of endogenous ARL3, as well as several other photoreceptor proteins, in serial tangential sections of the retina (Fig. 1D). In this technique, protein detection is based on western blotting (17,18), which makes it exempt from the tissue fixation artifacts, and it unambiguously confirmed that ARL3 is indeed present throughout the entire photoreceptor layer (Fig. 1D, sections 1–9). A significant fraction of ARL3 was present in the OS, where it co-localized with peripherin/RDS (Fig. 1D, sections 1–2). ARL3 enrichment was also observed in the IS domain that harbors mitochondria, which is adjacent to the connecting cilium, as evident from the presence of the mitochondrial marker, COX I (Fig. 1D, section 3). The low spatial resolution of this technique, however, did not allow us to conclude whether ARL3 is particularly enriched in the connecting cilium. Overall, immunofluorescence data and serial section analysis suggest that transgenic ARL3-Q71L and endogenous ARL3 are found throughout the rod photoreceptor layer including the OS.

Progressive loss of rod photoreceptor function in ARL3-Q71L mice

To examine the impact of expressing dominant negative ARL3 on the functioning of photoreceptor cells, we performed electroretinography (ERG) starting from PN20. Transgenic negative littermate controls show a robust 'a' wave indicative of photoreceptor function and 'b' wave demonstrating an appropriate response from downstream bipolar cells. A similar response was observed in animal models expressing ARL3-Q71L at light intensities under both scotopic and photopic conditions (Fig. 2A). This result indicates that the initial development and function of photoreceptor cells appear unaffected by the expression of ARL3-Q71L. However, there is a progressive loss of rod function and by PN70 scotopic a-wave amplitude is almost completely lost with slightly reduced photopic b-wave amplitude (Fig. 2A and B).

Rod photoreceptor cells degenerate in animals expressing ARL3-Q71L

Loss of photoreceptor function at PN70 could be due to photoreceptor cell death or defects in the phototransduction cascade. To distinguish these possibilities, we investigated the survival of photoreceptor cells by counting the outer nuclei at various ages of retinal development. At PN30, when there was a substantial reduction in rod photoresponse [463 ± 9 µV: Tg (–) versus 327 ± 56 µV: Tg (+); $P = 0.01$ Figure 2B], we observed no significant loss in photoreceptor cells. However, by PN70, most of the photoreceptor nuclei was lost in transgenic ARL3-Q71L animals compared with controls. The ONL length was measured at superior and inferior regions of the retina and was not significantly different at PN30, but was dramatically reduced in transgenic animals by PN70 [Tg(+) = 2.7 layers and Tg(–) = 10.3 layers; $P < 0.001$ at all locations, Figure 2D].

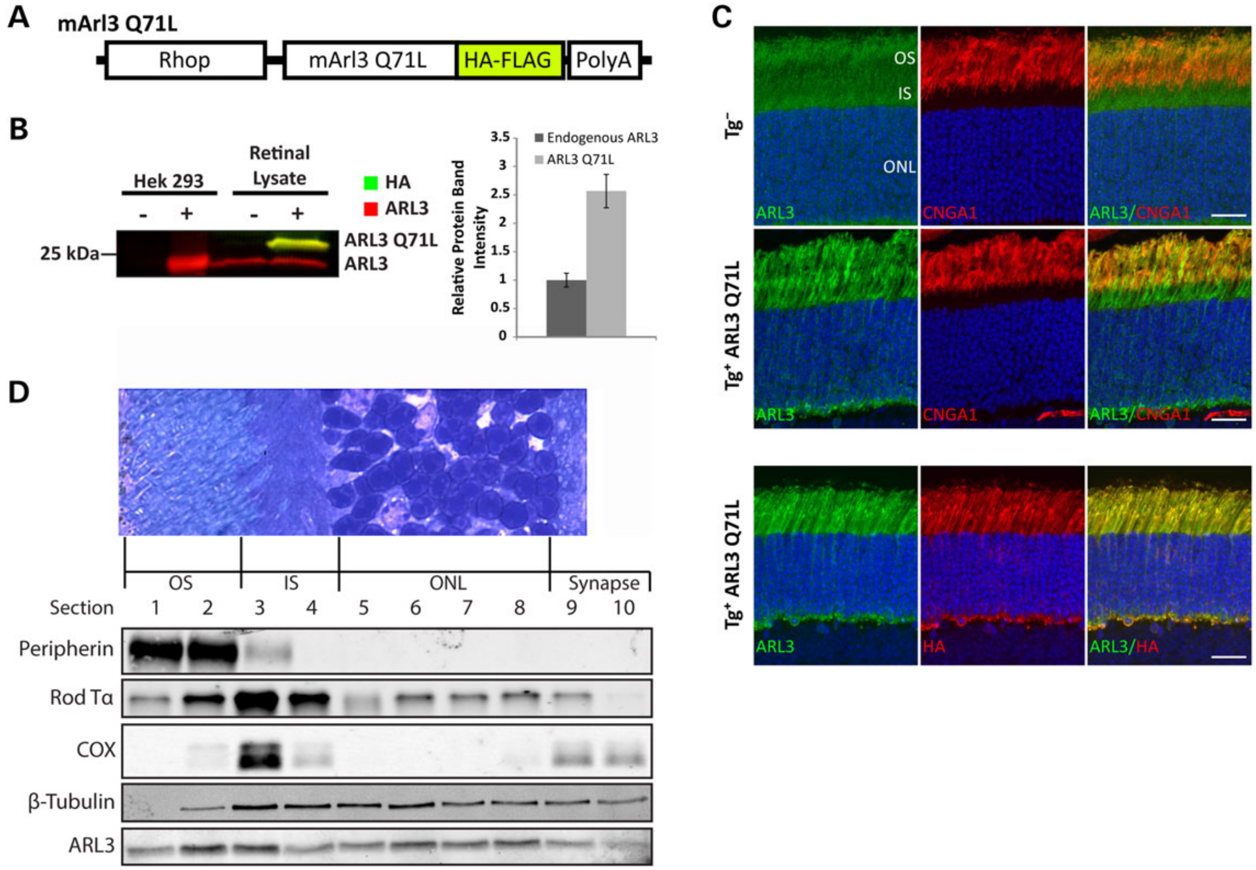

Figure 1. ARL3-Q71L dominant active mutant transgenic model generation. (**A**) Scheme showing the construct used to express ARL3 in rod photoreceptors cells. The *Arl3*-Q71L (glutamine to leucine) dominant active mutant was expressed under a 4.4 kb rhodopsin promoter. This mutant protein was also C-terminally tagged with FLAG and Hemagglutinin (HA). (**B**) Western blot analysis of HEK 293 cells transfected with empty vector or wild-type ARL3 (lanes 1 and 2) and retinal lysate from Tg(–) and Tg(+) ARL3-Q71L animals (lanes 3 and 4). Staining was done with antibodies directed at ARL3 (red) and HA (green) to compare expression levels of transgenic versus endogenous ARL3 (refer to bar graph; $P < 0.001$). (**C**) Retinal sections from Tg(–) and Tg(+) animals stained for ARL3 (green) and CNGA1 (red) (top and middle panel) and ARL3 (green) and HA (red) (bottom panel). (Scale bar = 10 µm.) (**D**) Representative immunoblots showing the distribution of ARL3 and other proteins in a set of serial tangential 10 µm sections (1–10) of the mouse retina. RDS (perpherin) was used as a rod OS marker, COX I was used as a mitochondrial marker present in rod IS and synapse, the α subunit of rod transducin (rod Tα) was used as a general rod marker and β-tubulin was used as a general cellular marker. The inset on top, showing a mouse retinal section stained with toluidine blue, is provided to illustrate the origin of each section from various cellular compartments of rod photoreceptors.

Normal elaboration of photoreceptor OS in ARL3-Q71L mice

The morphology of rod photoreceptor cells, in particular the structure of photoreceptor OS, was analyzed by light and electron microscopy at PN20, when the ERG responses appear normal. Gross morphology using toluidine blue staining on semi-thin sections show normal elaboration of photoreceptor OSs (Fig. 3A). The OS length of the rod photoreceptors in transgenic animals expressing ARL3-Q71L was comparable to that of transgenic negative littermate controls (Supplementary Material, Fig. S2A and B; OS length: Tg(+) = 11.54 ± 0.12 µm and Tg(–) = 11.66 ± 0.10 µm; $P = 0.39$). However, ultrastructural analysis revealed subtle defects including a slight increase in endosome content within the IS (Fig. 3B; white arrowheads) and misoriented rod OS discs (Fig. 3C; white arrows). The Golgi apparatus and endoplasmic reticulum appear dilated in the retina from ARL3-Q71L transgenic animals (Fig. 3C; Golgi apparatus = black arrows and ER = black arrowheads). These data suggest that overall development of photoreceptor cell OSs appears to be relatively normal; however, ultrastructural changes in both rod inner and OSs are present due to transgenic expression of ARL3-Q71L.

Expression of ARL3-Q71L reduces the levels of prenylated phototransduction proteins

The decrease in photoreceptor function despite normal morphology at PN30 suggests that expression of ARL3-Q71L might affect the levels of proteins that participate in phototransduction. In addition, previous *in vitro* studies suggest a relationship between ARL3 and prenylated proteins through its regulation of PrBPδ (10,11). Therefore, we investigated the levels of prenylated phototransduction proteins prior to significant degeneration at PN30. Prenylated phosphodiesterase catalytic subunits α and β (PDE6αβ) were reduced by ~50% in rod photoreceptor cells expressing ARL3-Q71L compared with controls (Fig. 4A and B; $P < 0.001$). Similarly, farnesylated G-protein receptor kinase (GRK1) and transducin γ (Tγ) levels in retina from ARL3-Q71L animals were reduced by ~40% and ~15%, respectively, compared with controls (Fig. 4A and B; GRK1, $P = 0.001$; Tγ, $P = 0.001$). It is important to note that GRK1 is expressed in both rods and cones. Since our animal model expresses ARL3-Q71L exclusively in rods, it is likely that the reduction in GRK1 in rods as tested by western blot is an underestimate. Additionally, other non-prenylated OS proteins remained unchanged including GC1, rod Tα and rhodopsin ($P > 0.05$) as well as rod arrestin (data not shown).

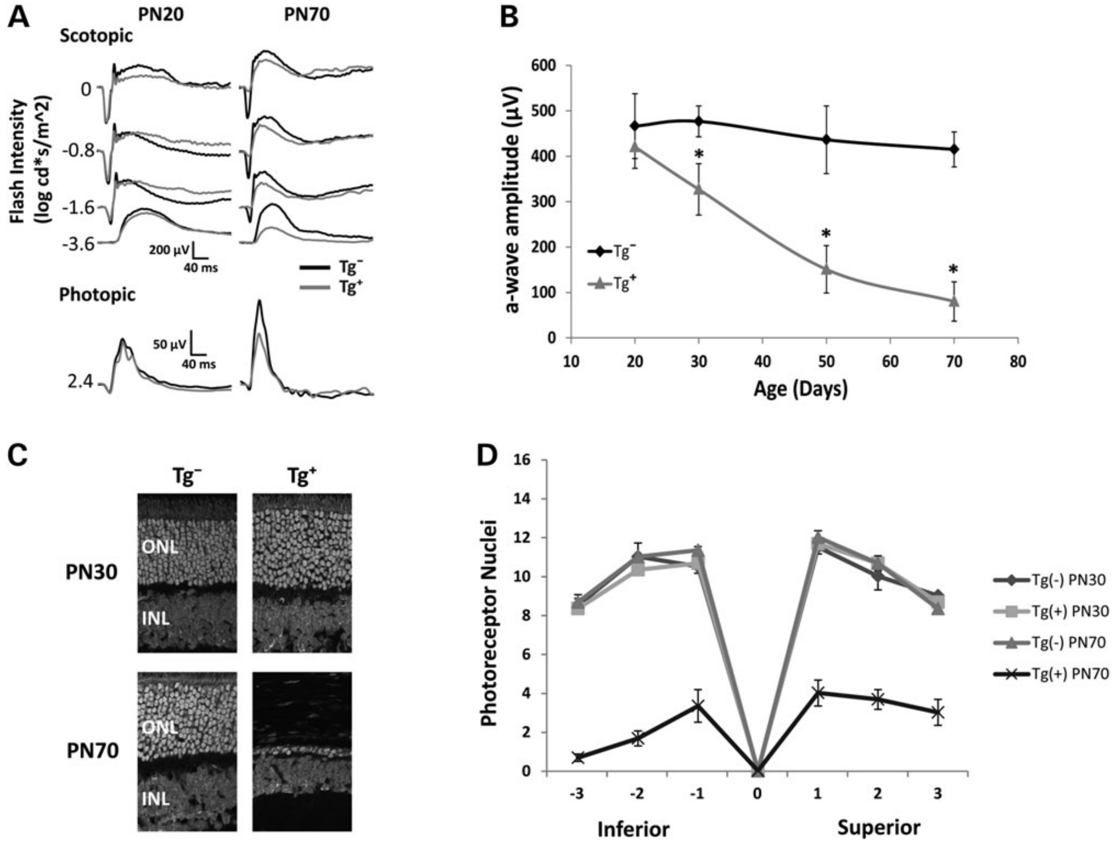

Figure 2. Progressive loss of rod photoreceptor function and degeneration in ARL3-Q71L retina. (**A**) Representative scotopic (rod) and photopic (cone) electroretinograms (ERGs) comparing Tg(−) and Tg(+) animals at PN20 and PN70 across multiple light intensities. (**B**) Graph illustrating the scotopic a-wave amplitude measured at the light intensity of 0 Log Cd*s/m^2 as a function of age. (**C**) Retinal sections showing nuclei from Tg(−) and Tg(+) animals stained with propidium iodide at PN30 and PN70. (**D**) Quantification of the ONL length (number of cell layers) at different locations within the retina from the inferior to superior portion between Tg(−) and Tg(+) animals at PN30 and PN70. *$P < 0.01$.

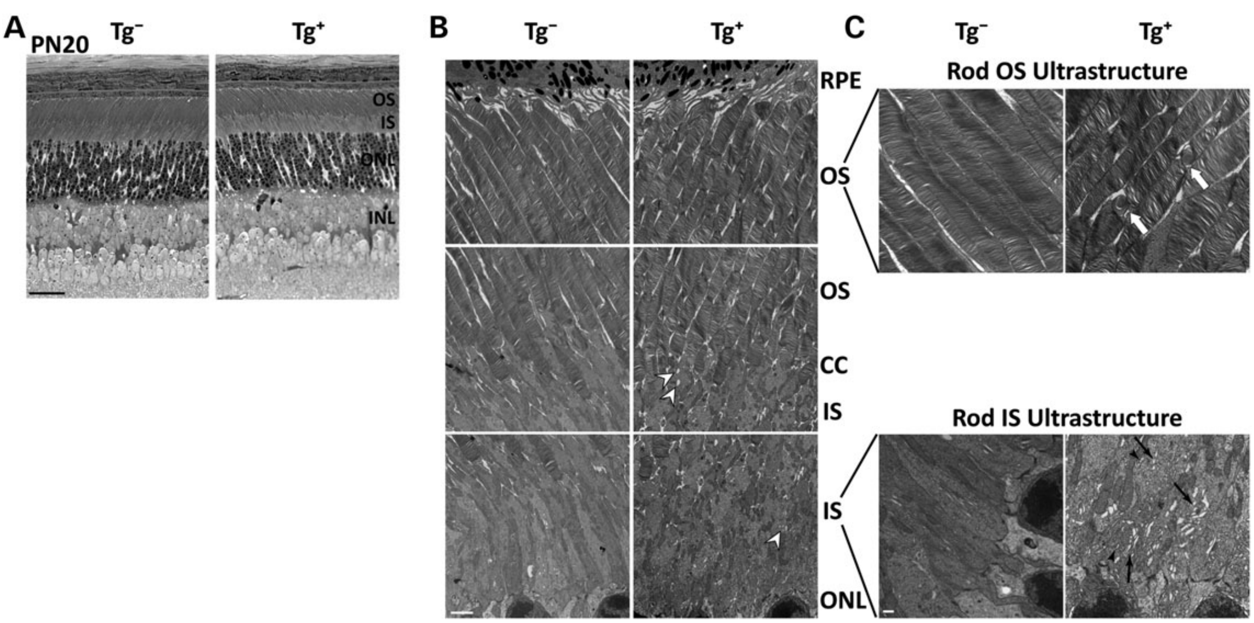

Figure 3. Normal elaboration of photoreceptor OS in ARL3-Q71L Mice. (**A**) Semi-thin sections of Tg(−) and Tg(+) retina from PN20 littermates stained with toluidine blue (scale bar = 20 µm). (**B**) Low magnification images from the OS and IS with endosomes indicated by white arrowheads (scale bar = 2 µm). (**C**) High magnification ultrastructure of the OS. White arrows point to membrane whorls in the rod OS from Tg(+) retina. Dilated endomembranes in the rod IS including Golgi apparatus indicated by black arrows and rough endoplasmic reticulum indicated by black arrowheads (scale bar = 0.5 µm).

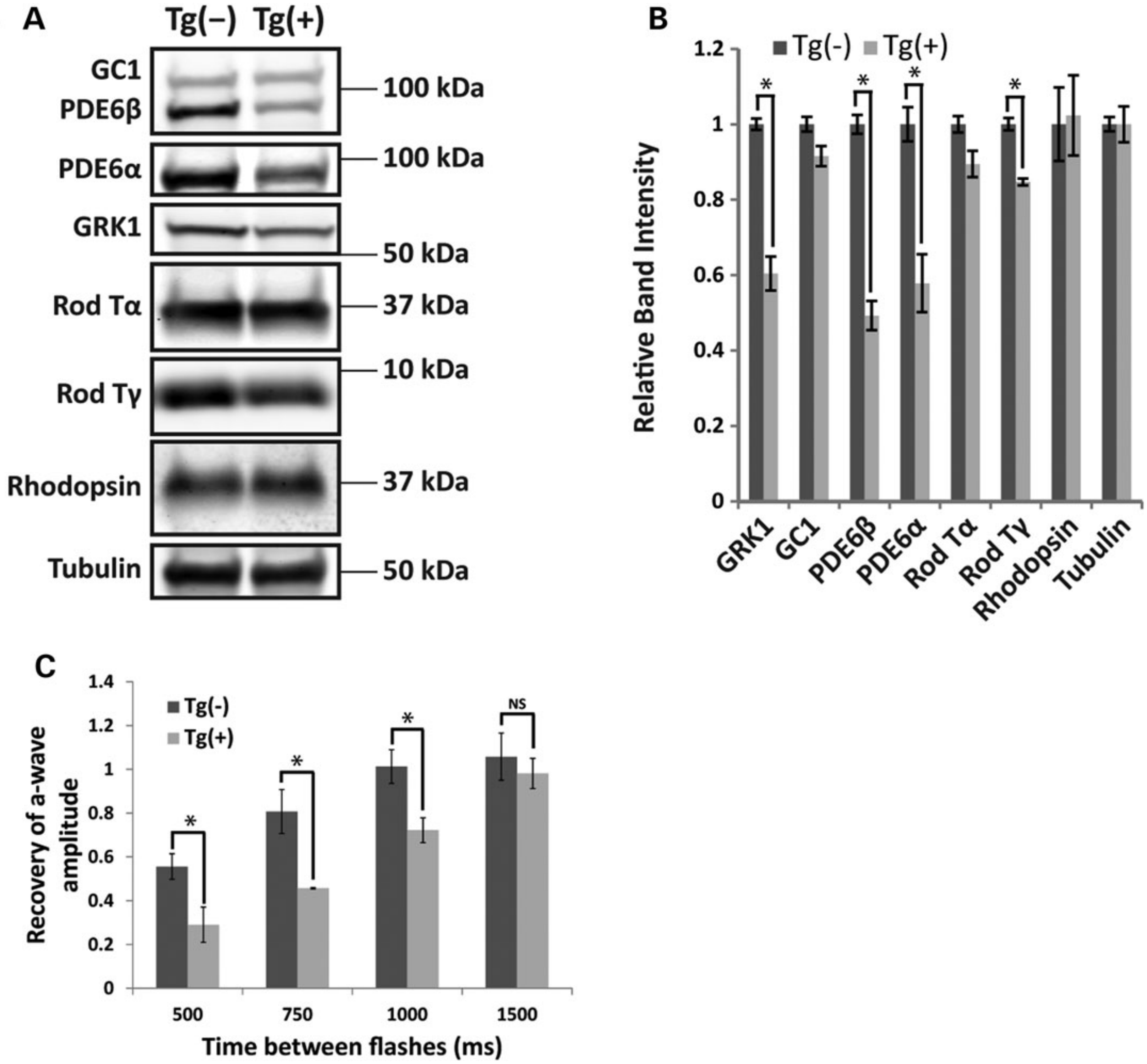

Figure 4. Expression of ARL3-Q71L reduces the levels of prenylated phototransduction proteins. (**A**) Representative immunoblots of PN30 retinal protein samples showing levels of prenylated OS proteins and non-prenylated controls. (**B**) Quantification of protein levels from Tg(–) and Tg(+) retinal isolates (PDE6β : $P = 0.0004$, PDE6α : $P = 0.009$, GRK1 : $P = 0.001$, Tγ : $P = 0.001$). (**C**) Scotopic double flash (recovery) at PN20 shows the recovery of a-wave amplitude at different latencies between flashes from Tg(–) and Tg(+) animals (500 ms, $P < 0.002$; 750 ms, $P < 0.001$; 1000 ms, $P < 0.002$; 1500 ms, $P = 0.32$). Asterisk indicates statistically significant difference.

Phosphorylation of activated opsin mediated by GRK1 is necessary for the recovery of photoresponses following a flash of light (19–21). In order to determine if there is a functional loss of GRK1, scotopic double flash (recovery) experiments were done that involve dark-adapting the animal and subsequently administering two sequential low intensity (−1.6 Log cd s/m^2) flashes (the test flash and the probe flash) with various delays between the two flashes. This provides insight into how quickly rod photoreceptors can recover to produce the same response as the test flash. As expected from the reduction in GRK1, recovery of scotopic a-wave was reduced in ARL3-Q71L mice at PN20 compared with controls (Fig. 4C). The scotopic a-wave was completely recovered (i.e. probe flash = test flash) after a 1500 ms in ARL3-Q71L animals compared with controls in which complete recovery occurred at a 1000 ms delay (Fig. 4C). Overall, these data demonstrate that ARL3-Q71L expression results in a specific reduction in prenylated proteins that more severely affects PDE6 and GRK1 than Tγ but does not affect other non-prenylated OS proteins.

Loss of rod GRK1 and mislocalization of PDE6 in ARL3-Q71L mice

After verifying that transgenic expression of ARL3-Q71L caused a specific effect on prenylated protein levels, the localization of those proteins was assessed by immunofluorscence microscopy at PN25 prior to significant cell death. Two distinct defects were noted with respect to different prenylated proteins. In agreement with our results from immunoblotting, we found a marked reduction in immunoreactivity for GRK1 in the rod OS in transgenic ARL3-Q71L animals. As expected, expression of GRK1 in cone OSs was unaffected (Fig. 5A). Interestingly, transgene expression resulted in mislocalization of PDE6 subunits, and to a lesser extent transducin, to the IS in large punctate structures (Fig. 5A–E). Similar to our Tg(–) littermate controls, immunoreactivity of PDE6β in Tg(+) ARL3-WT was exclusively found in the OS (Supplementary Material, Fig. S1). In addition, other non-prenylated OS proteins were properly localized with comparable intensity, including cyclic nucleotide gated channel α1 (CNGA1) (Fig. 5B–E) and peripherin (Fig. 5A) as well as rhodopsin and GC-1 (data not shown).

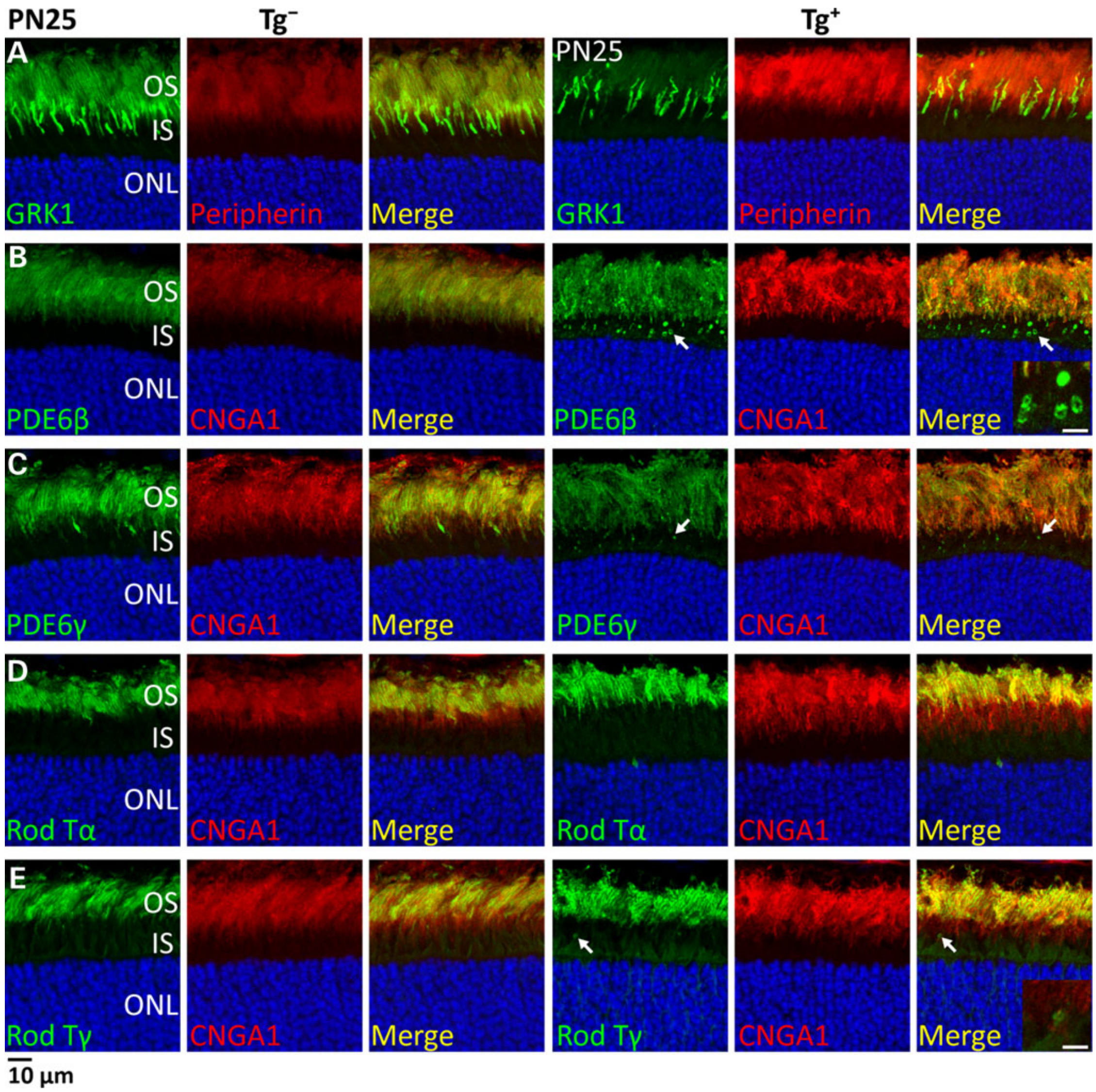

Figure 5. Loss of rod GRK1 and mislocalization of PDE6 in ARL3-Q71L mice. Immunolocalization of OS proteins in retinal cross-sections at PN25. (**A**) GRK1 (green) counterstained with peripherin/RDS (red) in Tg(−) and Tg(+) sections. (**B**) PDE6β (green) and (**C**) PDE6γ (green) each counterstained with CNGA1 (red) in Tg(−) and Tg(+) sections. Mislocalization of PDE6β or PDE6γ is indicated by white arrow. Inset in (B) shows a cropped and zoomed image (scale bar = 5 μm) of large punctate structures immunoreactive for PDE6 (ranging from 0.5 to 2 μm in diameter) within the inner segment. (**D**) Rod Tα (green) and (**E**) Rod Tγ (green) counterstained with CNGA1 (red) in Tg(−) and Tg(+) sections. White arrow indicates mislocalized transducin in the IS.

Furthermore, the punctate structures with immunoreactivity for PDE6 and transducin progressively accumulate with age (Fig. 6A, b). This accumulation of PDE6 in the IS corresponds to a decrease in levels of PDE6 in OS. Additionally, the PDE6 found in these structures is likely assembled as it was identifiable with the anti-ROS1 antibody, which is known to recognize only the assembled PDE6 complex (PDE6αβγ) (22). This assembled PDE6αβγ was colocalized on the same IS structures as transducin (Fig. 6B). Overall, the data suggest that transgenic expression of ARL3-Q71L results in mislocalization and degradation of prenylated OS proteins.

Accumulation of endosomal vesicles in the retina expressing ARL3-Q71L

To explore the ultrastructural defects, electron microscopy was performed at PN30 prior to significant cell death at which point accumulation of PDE6 in IS was observed. As expected, general retinal morphology was maintained as shown by semi-thin sections stained with toluidine blue (Fig. 7A). Notably, we observed Muller cell processes extending into the IS through the outer limiting membrane (Fig. 7C; Muller cell = MC). Furthermore, endosome-like structures and misoriented or disrupted OS along with membranous whorls within the IS were frequently observed in PN30 transgenic animals (Fig. 7B and C; top three rows; IS membrane whorls = asterisk, endosomes = white arrowheads, disrupted OS = white arrow). The endosome-like structures tended to be between 1 and 2 μm in diameter, which is comparable to the size of the punctate PDE6-containing structures identified by confocal IHC microscopy, suggesting that the prenylated proteins may be localized to endosomal compartments (Fig. 7D; PDE6 panel 1 compared with endosome-like structures (panels 2, 3, 4, 6) and IS membrane whorl (panel 5). Additionally, in ARL3-Q71L animals, the frequency of misoriented/disrupted OS membrane discs was higher and there were fewer well-oriented OSs compared with controls likely resulting from initial stages of photoreceptor cell death (Fig. 7C, top row; white arrows). In

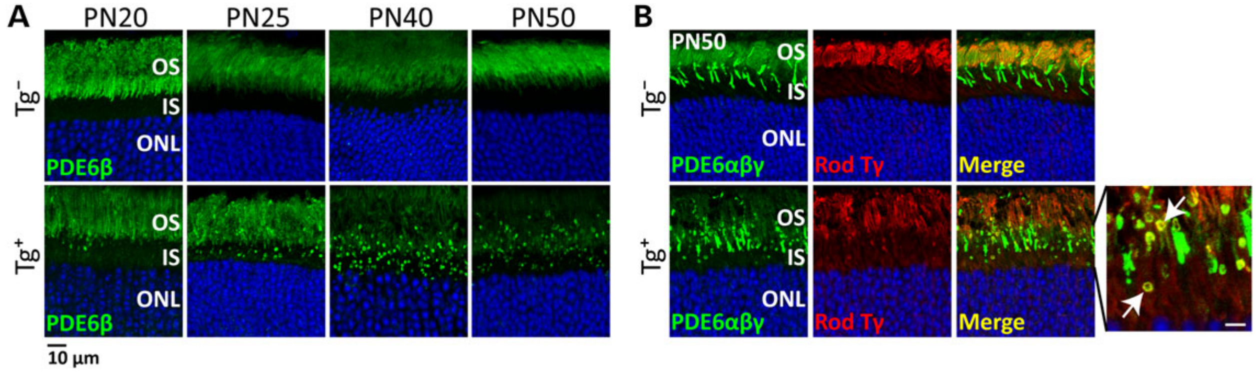

Figure 6. Progressive accumulation of rod PDE6 and colocalization of assembled rod PDE6 with GRK1 and transducin. (**A**) Immunolocalization of PDE6β in retinal cross-sections of Tg(−) and Tg(+) tissues from various ages (PN20–PN50). (**B**) PDE6αβγ (identified by ROS1 antibody), rod Tγ (Top Panel: red) immunolocalization in Tg(−) and Tg(+) retinal cross-sections at PN50. Zoomed image on right illustrates colocalization of PDE6αβγ with Tγ with PDE6αβγ in IS punctate structure indicated by white arrow (scale bar = 3 µm).

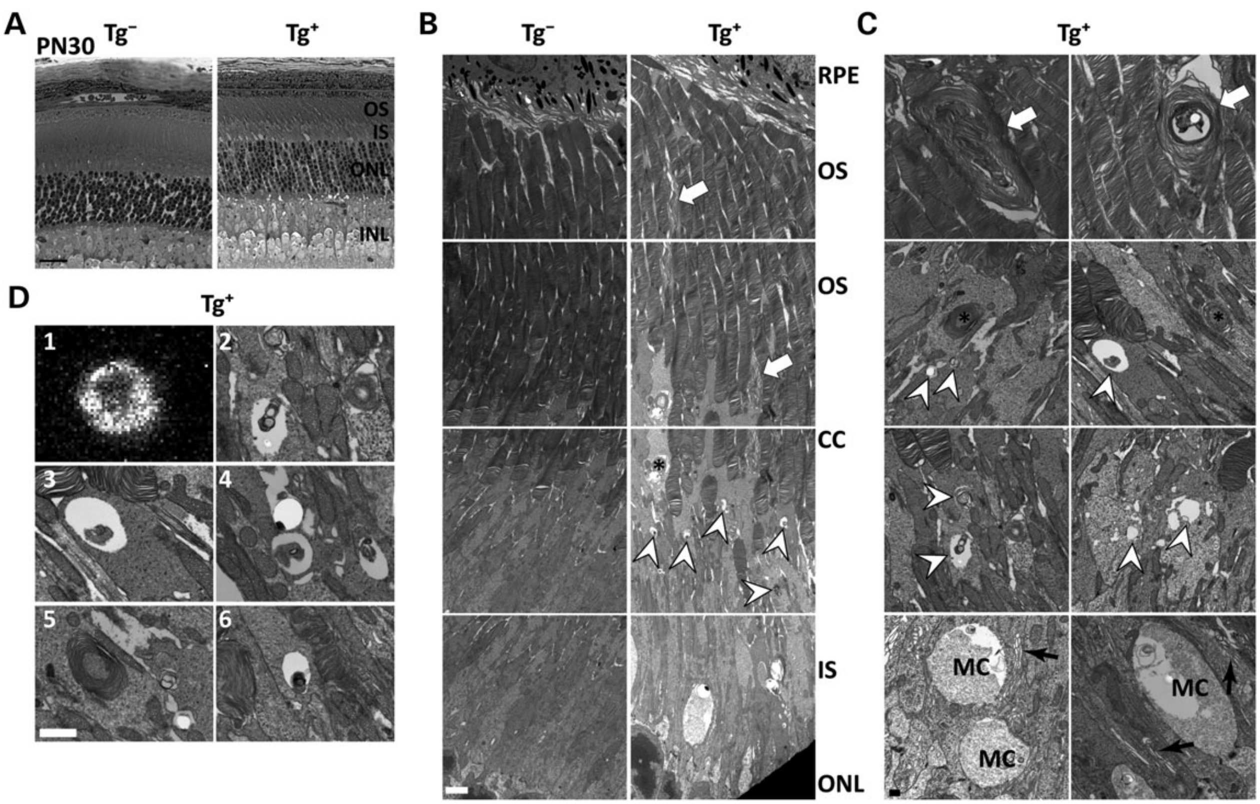

Figure 7. Accumulation of endosomal vesicles in the retina expressing ARL3-Q71L. (**A**) Semi-thin toluidine stained retinal sections from Tg(−) and Tg(+) animals at PN30 (scale bar = 20 µm). (**B**) Electron micrographs at low magnification illustrating the structural abnormalities of the photoreceptor OS and IS in Tg(+). Littermate Tg (−) serves as the control. Increased frequency of endosomes (white arrowhead), IS membrane whorls (*) and mis-oriented/dysmorphic OS discs (white arrow) (scale bar = 5 µm). (**C**) Electron micrographs from Tg(+) retina displaying high magnification images of the structures from (B) (top 3 rows) as well as dilated Golgi apparatus (black arrows) and Muller glial cells extending through the outer limiting membrane (MC) (scale bar = 0.5 µm). (**D**) Comparison of immunofluorescent punctate structure with PDE6β immunoreactivity on the same scale as the high magnification electron micrographs of the abnormal structures in the IS (scale bar = 1 µm).

conclusion, drastic ultrastructural changes were found in ARL3-Q71L mice, including mislocalized prenylated proteins likely to be accumulating in endosome-like structures within the IS.

PrBPδ interacts with ARL3 *in vivo*

To provide mechanistic insight into the defects seen in the ARL3-Q71L transgenic animals, we performed co-immunoprecipitation (co-IP) experiments. We utilized the HA tag to pull-down ARL3-Q71L protein in retinal lysates from transgenic animals. Based on *in vitro* binding data, we expected that constitutively active ARL3-Q71L would trap PrBPδ, and thus disable it (10,23). Here, we have for the first time shown that ARL3-Q71L co-immunoprecipitates PrBPδ *in vivo* while transgenic tagged ARL3-WT does not (Fig. 8). Moreover, we show that PDE6 does not interact with ARL3-Q71L or ARL3-WT (Fig. 8). This indicates that when

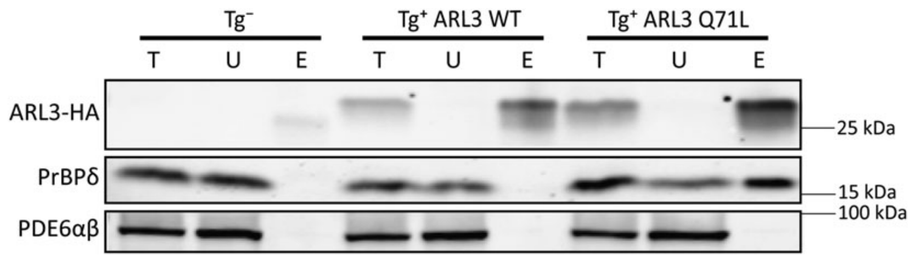

Figure 8. PrBPδ interacts with ARL3-Q71L *in vivo*. Immunoprecipitation (IP) of retinal isolates from Tg(−), Tg(+) ARL3-WT (middle) and Tg(+) ARL3-Q71L (right) using rat monoclonal antibody against HA tag. Following IP, immunoblots were probed with indicated antibodies. T = Total, U = Unbound and E = Eluate.

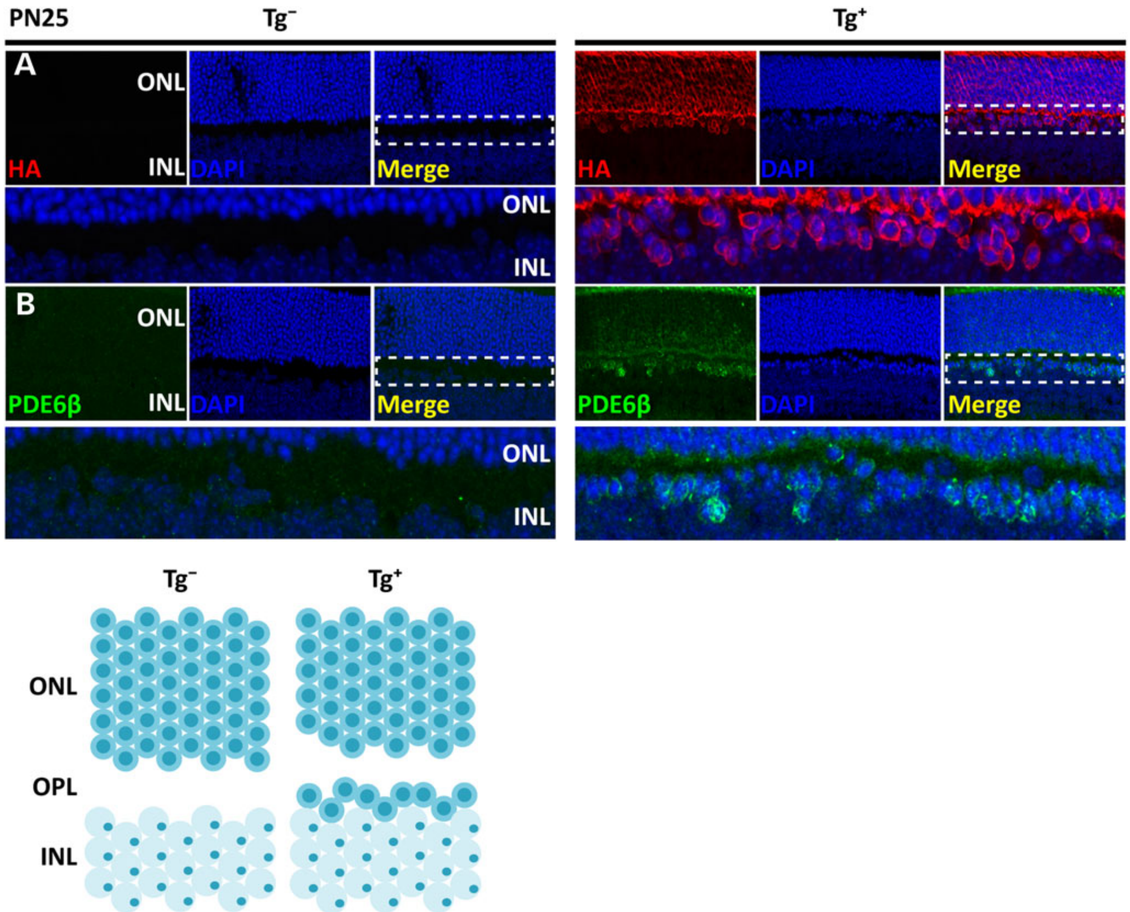

Figure 9. Defective migration of rod photoreceptor cells in ARL3-Q71L retina. (**A**). Retinal cross-sections stained for HA (red) and DAPI (blue) comparing Tg(−) littermate and Tg(+) tissues at PN25. The zoomed image below was cropped from the white dashed box in the merge image above. (**B**). Retinal cross-sections stained for rod-specific PDE6β (green) and DAPI (blue) comparing Tg(−) and Tg(+) tissues at PN25. The diagram below illustrates the observed migration defect in transgenic animals expressing ARL3-Q71L.

ARL3-Q71L is bound to PrBPδ it does not bind PDE6, which is consistent with previous studies suggesting that ARL3 causes release of prenylated cargo like PDE6 (24).

Defective rod photoreceptor cell migration in ARL3-Q71L retina

The retina is normally laminated such that the ONL contains only rod and cone photoreceptors and the INL consists of downstream neurons (e.g. bipolar cells). Unexpectedly, we observed a defect in rod photoreceptor cell migration in ARL3-Q71L expressing retina. The migration defect was uniformly observed across the retina (data not shown). More specifically, a fraction of rod photoreceptor cells, indicated by HA (red) and PDE6 (green) staining, were located in the INL/OPL in adult tissues (Fig. 9A–B). DAPI staining further confirms the identity of these cells as chromatin of rod photoreceptor cells are distinctly more dense compared with downstream neurons (25,26). It should be noted that there was varying severity between different founder lines and the severity of the defect corresponded to the level of transgenic protein expression. For photoreceptor migration experiments, the highest expressing line was characterized, which showed a more dramatic mislocalization of photoreceptor nuclei than other founder lines. Overall, these data suggest that ARL3 plays an important role in the migration of rod photoreceptor cells.

Discussion

Regulation and rapid movement of proteins from the photoreceptor inner to OS is a poorly understood process and is of clinical significance as defects in this protein trafficking lead to blindness. Due to changes in conformation dependent on nucleotide binding, small GTPases are ideally suited for polarized movement of proteins. In this study, we examined the role of ARL3, a small GTPase, in the trafficking of proteins to the rod photoreceptor OS. In addition, mutation or depletion of RP2 associated with XLRP in humans likely results in excess active (GTP-bound) ARL3, similar to the animal model described in this study (7,13). Therefore, our animal model is also useful in understanding the pathogenesis underlying the defects in RP2-associated diseases. In the current study, we show that expression of constitutively active ARL3 (ARL3-Q71L) results in progressive loss of function and degeneration of rod photoreceptor cells. The decline in photoreceptor function was accompanied with progressive accumulation of prenylated PDE6 and transducin in IS. Moreover, levels of farnesylated GRK1 were dramatically reduced. Our study establishes the role of ARL3 in trafficking and stability of prenylated proteins in rod photoreceptor cells.

Importantly, the phenotypes associated with ARL3-Q71L were specific to ARL3 function and not a result of overexpression or transgene insertion as the loss of photoreceptor function corresponded to the level of ARL3-Q71L expression between multiple independent founder lines (Supplementary Material, Fig. S3). The number of PDE6 containing vesicles in the IS also corresponded to the level of transgene expression (Tg(+++) 11.4 ± 0.9 vesicles/1000 μm^2 and Tg(++) 2.8 ± 0.2 vesicles/1000 μm^2; $P = 0.01$; data not shown). In addition, the defects observed in ARL3-Q71L animals were specific as these were not observed in transgenic animals expressing ARL3-WT (Supplementary Material, Fig. S1) or ARL2-Q70L (Z.C.W. and V.R., unpublished data).

Prior to degeneration, we observed no changes in levels or localization of major photoreceptor OS proteins except for prenylated proteins in the ARL3-Q71L transgenic animals. More specifically, levels of PDE6 and GRK1 were severely decreased while transducin levels showed modest reduction at one month old. Immunofluorescence data suggested that these prenylated proteins are trafficked normally to the OS initially, but as the animals aged mislocalization to the IS became more severe. These prenylated proteins accumulated in punctate structures in the IS and the number of these structures increased with age. It should be noted that these structures did not colocalize with the Golgi marker, GM130 and therefore are not Golgi dilations (unpublished data). TEM analysis showed that ARL3-Q71L expression induced endosomal-like structures within the photoreceptor IS, and we hypothesize that misrouted OS proteins were packaged within these structures. The size of the fluorescent puncta identified via immunofluorescence was estimated between 1 and 2 µm in diameter, which corresponded to the large endosomal structures frequently found in the IS of TEM sections (Fig. 7). It is likely that prenylated proteins accumulate on the membrane of endosomes due to their lipid modification. This assumption is corroborated by immunofluorescence data, which shows large punctate structures with staining on the circumference of the spherical structure with absent staining in the middle. In addition, staining of these endosomes with the ROS-1 antibody, which recognizes the PDE6αβγ complex and not individual subunits, suggests that PDE6 is in fact fully assembled. Importantly, assembled PDE6 and rod transducin γ were present on the same puncta within the IS and the number of these puncta increased as the animal aged. Altogether, our results suggest that these prenylated proteins translocate to the OS via a trafficking pathway that is dependent upon proper function of ARL3, and over-activation results in buildup of these proteins in the same subcellular compartment that ultimately leads to their degradation.

How does ARL3 over-activation result in specific trafficking defects in prenylated proteins? We show that active ARL3-Q71L interacts with PrBPδ while ARL3-WT does not. Although the PrBPδ homolog, UNC119, has been identified as an interacting partner of ARL3 *in vitro* (9,23), we do not see this interaction in our system. The reason behind this observation is not clear. It is possible that the affinity for UNC119 for ARL3-Q71L is lower and therefore below the detection sensitivity in our experimental system. Our results suggest that mistrafficking of prenylated proteins is due to the sequestration of PrBPδ as well as its homologs by the dominant active ARL3-Q71L. For PrBPδ, this would result in a predominant 'closed' conformation and loss of the ability to bind prenylated proteins. The mislocalization of prenylated proteins in ARL3-Q71L expressing mice is also in agreement with findings from knockout of PrBPδ or RP2, the GAP for ARL3 (7,12,14).

Photoreceptor degeneration in this ARL3-Q71L mouse model is rapid and nearly complete by PN70. The primary cause of the rapid photoreceptor loss is the ability of ARL3 to sequester multiple binding partners including PrBPδ due to defective GTP hydrolysis by ARL3-Q71L. In addition to its potential role in prenylated protein trafficking, ARL3 is also thought to participate in the regulation of dynein motors, Golgi maintenance and vesicle dispersion and microtubule stability (16,27–32). However, we observed normal trafficking of non-prenylated proteins suggesting that dynein motors and microtubules are not affected. A moderate Golgi and ER dilation was noted specifically in transgenic animals. We believe this is due to the excessive accumulation of prenylated proteins in the endomembrane system as they cannot be properly retrieved by PrBPδ or its homologs. Further studies are needed to test this hypothesis.

Surprisingly, we observed defective migration of a fraction of ARL3-Q71L expressing photoreceptor cells. These cells remained in the INL and in the OPL instead of migrating to the ONL. It is likely only a fraction of photoreceptor cells express ARL3-Q71L prior to migration since expression under the 4.4 kb rhodopsin promoter is detectable at PN4 (15) while the majority of photoreceptor nuclei have migrated to the outer layer by PN6 (33). Interestingly, defective migration of nuclei is also present in mice lacking RP2 where ARL3 is thought to be overactive (13; Fig. 4). We hypothesize that this migration defect results from instability or improper localization of the farnesylated lamins. Depletion of lamins results in neurodevelopmental phenotypes, including a severe defect in neuronal migration and nuclear abnormalities such as blebs and elongation (34,35). Similarly, we observed blebs in the nuclear envelope (Supplementary Material, Fig. S4). Additionally, it was recently found that PrBPδ interacts with lamin B (36). Alternatively, ARL3 has been shown to affect cytokinesis through a microtubule function-based mechanism which could ultimately affect proper lamination of photoreceptor cells (30). Importantly, ARL3 is ubiquitously expressed throughout different tissues including the brain (37), suggesting that it could be involved in the process of neuronal migration in the CNS. Disruption of this process results in lethal and non-lethal neurodevelopment defects including lissencephaly, epilepsy,

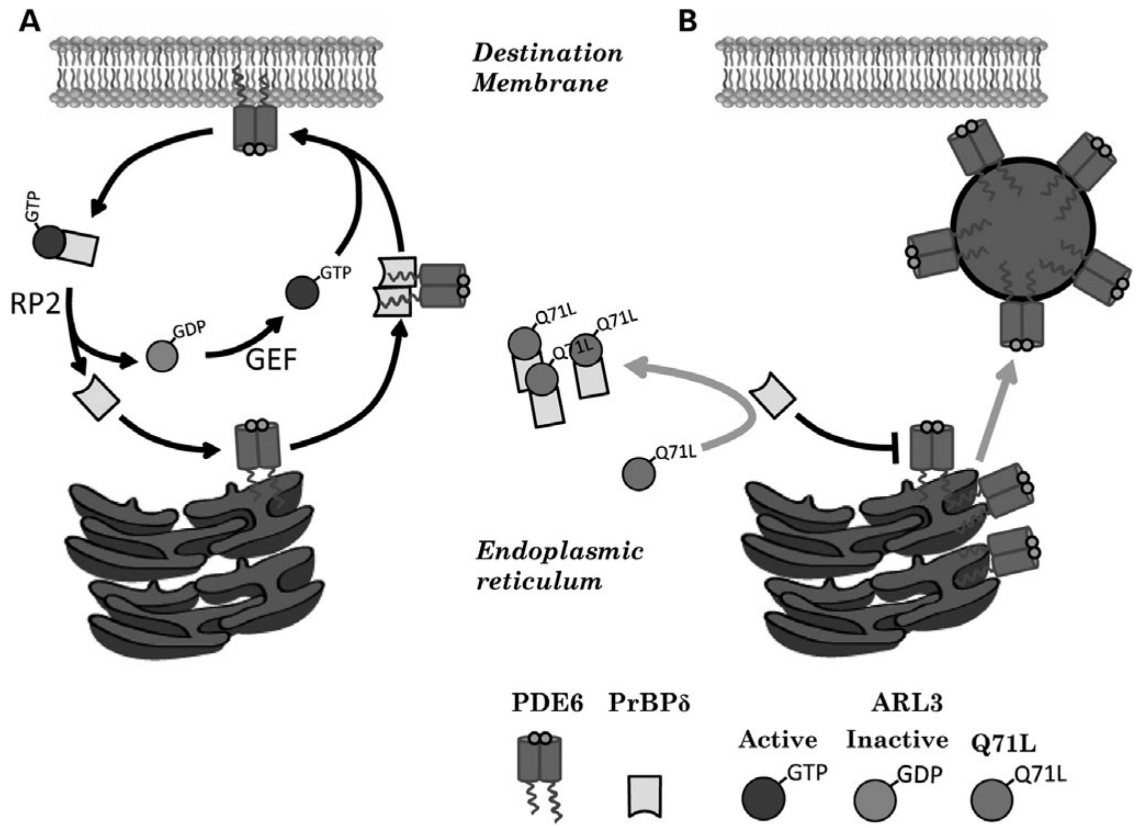

Figure 10. Mechanistic model for mistrafficking of prenylated proteins in ARL3-Q71L mouse. (**A**) After prenylation and further processing, PDE6 and GRK1 are peripherally bound to the ER membrane. PrBPδ, or its homologs, extract prenylated proteins from the endomembrane and target them to the destination membrane. ARL3 is activated by its GEF (ARL13b) in the area of the destination membrane and binds to PrBPδ causing release of PDE6 and/or GRK1. RP2 accelerates the GTPase activity of ARL3 stimulating release of PrBPδ from the PrBPδ–ARL3–GTP complex. (**B**) Exogenously expressed active ARL3-Q71L sequesters PrBPδ and its homologs, thereby rendering it in capable of extracting PDE6 from the ER membrane. PDE6 and other prenylated proteins buildup in the ER membrane and are pushed out of the ER in endosomal vesicles which accumulate in the IS.

schizophrenia and autism (38–41). In conclusion, this novel ARL3 function has broad implications in neuronal migration and associated disease, and therefore requires further research.

Based on the results obtained in this study, we have developed a mechanistic model of ARL3 function in rod photoreceptor cells and how this mechanism goes awry in the presence of a dominant active ARL3 mutant (Fig. 10). After addition of a prenyl group by a specific prenyl transferase, prenylated proteins such as PDE6, GRK1 and transducin are targeted to ER as the last two steps of prenyl processing, endoproteolysis and methylation, are mediated by ER-membrane bound enzymes. How these prenylated proteins are then moved to the OS from the ER compartment still remains a mystery. Based on our results and previous studies, we believe that PrBPδ and its functional homologs can retrieve the prenylated proteins from the ER membrane for further transport to the destination membrane similar to the proposed transport of K-ras from the ER to the plasma membrane (42,43). This process must be regulated by ARL3 such that the proteins are selectively released at the appropriate location. In order for this to occur, the recently identified GEF of ARL3, ARL13b (44), must be localized in the area of the destination membrane such that ARL3 can be activated and bind PrBPδ or its homolog causing release of the cargo protein, that is PDE6, GRK1 or transducin. Interestingly, recent research shows that ARL13b localizes to the cilium and OS region (45), which is corroborated by our results (Supplementary Material, Fig. S5). This finding suggests that ARL3-mediated release of cargo occurs at the cilium or in the OS. Additionally, the ARL3–PrBPδ complex can then be acted on by RP2, which facilitates hydrolysis of GTP to GDP thereby inactivating ARL3 and causing dissociation and recycling of PrBPδ and its homologs. In our dominant active transgenic ARL3-Q71L model, it is likely that this complex remains intact and sequesters PrBPδ from its transport cycle of prenylated proteins (Fig. 10b). Disruption of the transport of prenylated proteins results in their accumulation in IS and sorting to a degradation pathway.

Our study sheds light on the process of targeted protein transport and our current model shows the importance of ARL3 regulation in trafficking of prenylated phototransduction proteins. Finally, we believe our animal model mimics human XLRP resulting from RP2 mutations that disrupt the small GTPase cycle of ARL3.

Materials and Methods

Generation of ARL3-Q71L transgenic mice

Full-length mouse *Arl3* was amplified from a clone purchased from a commercial vendor (Thermo Scientific). Using polymerase chain reactions (PCR), we engineered a tandem C-terminal hemagglutinin (HA) and FLAG fusion tags and subsequently subcloned this PCR product behind a 4.4 kb *rhodopsin* promoter (Rhop) (15).

ARL3-Q71L dominant active mutant was constructed with the full-length tandem tagged *Arl3* as the template. A mutant oligonucleotide with specific change altering glutamine (Q) at position 71 to leucine (L) (WV832: 5′-TCT GAT TTT CCT CAG CCC GCC AAT GTC-3′) was used to create the *Arl3* mutant with the use of megaprimer directed site-directed mutagenesis method. The megaprimer was further extended and amplified using flanking primers containing *Sal*I and *Bam*HI restriction sites. The PCR product was then cloned behind 4.4 kb rhodopsin promoter using *Sal*I and *Bam*HI restriction sites. All clones selected were sequenced in both directions to confirm that there are no unintended mutations.

The plasmid backbone from clones containing *Rhop-Arl3* (wild-type) and *Rhop-Arl3- Q71L* (mutant) was removed by digestion with *Kpn*II and *Not*I enzymes and purified using agarose gel electrophoresis followed by elution of the fragment containing *Rhop-Arl3 (or Arl3-Q71L)-polyA*. The purified DNA fragment was injected into the pronuclei of oocytes from superovulated FVB/N females (WVU Transgenic Animal Core Facilities) and implanted into pseudo-pregnant CD-1 females.

Genotyping and founder line maintenance

Wild-type ARL3 (ARL3-WT) and mutant ARL3-Q71L transgenic founders were identified by PCR using either genomic DNA prepared from tail or ear punches: (5′ GGA TCG TGA ATC AGC CTC TGG CTT 3′; and 5′ TTT CTT CTT TGC GTT GAC ATT CTT GC 3′). All PCR reactions were conducted using NEB quick load *Taq* polymerase with following conditions, 95°C—2 min, 95°C—30 s, 59°C—30 s, 72°C—45 s with last three steps repeated for 33 cycles followed by a final extension step of 72°C at 5 min. Founders were backcrossed into wild-type 129/SV-E mice (Charles River) to eliminate the $Pde6b^{rd1}$ mutation present in the FVB founders. Removal of *rd1* allele was confirmed by PCR genotyping (46). The animals were maintained under 12 h light/12 h dark light cycles with food and water provided *ad libitum*. All experimental procedures involving animals in this study were approved by Institutional Animal Care and Use Committee of the West Virginia University.

ERG analysis

Mice were dark-adapted overnight prior to testing. Test subject eyes were topically dilated with a 1:1 mixture of tropicamide: phenylephrine hydrochloride. For ERG testing, mice were placed on a heated platform with continuous flow of isoflurane anesthesia through a nose cone [1.5% isoflurane with 2.5 liters per minute (lpm) oxygen flow rate]. A reference electrode was placed subcutaneously in the scalp. ERG responses were recorded from both eyes with silver wire electrodes placed on each cornea, with contact being made with a drop of hypromellose solution (2% hypromellose in PBS) (Gonioscopic Prism Solution, Wilson Ophthalmic, Mustang, OK, USA). Rod-dominated responses were elicited in the dark with flashes of LED white light at increasing flash intensities. Light-adapted cone responses were elicited with white light flashes in the presence of a 30 cd/m^2 rod-saturating white background light. ERGs were performed on the UTAS Visual Diagnostic System with Big-Shot Ganzfeld with UBA-4200 amplifier and interface, and EMWIN 9.0.0 software (LKC Technologies, Gaithersburg, MD, USA). Double flash ERG was performed just as above except to flashes were administered at −1.6 LogI for scotopic (rod) recovery and 2.4 LogI (under background light as above) for photopic (cone) recovery. The recovery (probe) flashes were elicited at variable delays after the initial (test flash) (500, 750, 1000 or 1500 ms after the test flash).

Generation of antibody against full-length ARL3

ARL3 protein was purified from pTriex-4 vector expressing a C-terminal his-tagged ARL3 protein in Origami *E.coli* strain (Novagen). Origami cells were grown to an $OD_{600} \approx 0.6$ and protein production was induced with 1 mM IPTG for 18 h at 18°C. Finally, the protein was purified from IPTG induced *E.coli* soluble fraction using a Nickel His Affinity Column and purified protein was supplied to Pacific Immunology Corp. for generation of the antibody in rabbits. The antibody serum was affinity-purified using a GST-ARL3 fusion protein. Purified antibody was then tested by western blot and immunofluorescence in HEK 293 cells expressing recombinant ARL3 and retinal extracts from animals expressing ARL3.

Immunoblots

Mice were euthanized by CO_2 inhalation and eyes were enucleated. For immunoblots, flash-frozen retinal samples were dissected from enucleated eyes and sonicated in phosphate buffered saline [PBS: 137 mM NaCl, 2.7 mM KCl, 4.3 mM $Na_2HPO_4 \cdot 7H_2O$, 1.4 mM KH_2PO_4, with protease inhibitor cocktail (Roche)]. Protein concentrations were measured using a NanoDrop spectrophotometer (Thermo Fisher Scientific, Inc.). Samples were loaded at 150 µg total protein per well of a 4–20% gradient polyacrylamide SDS–PAGE resolving gel (Criterion Midi format, Bio-Rad), resolved and transferred onto polyvinylidene difluoride membranes (Immunobilon-FL, Millipore, Billerica). Membranes were blocked with western blot blocking buffer (Rockland Inc.) for 30 min at room temperature and incubated with the indicated primary antibodies below overnight at 4°C. Blots were washed in PBST (PBS with 0.1% Tween-20) three times for 5 min each wash (3 × 5 min) at room temperature and incubated in secondary antibody, goat anti-rabbit Alexa 680 (or 800), goat anti-rat Alexa 800 or goat anti-mouse Alexa 680 (Invitrogen) for 30 min at room temperature. After 3 × 5 min of washes with PBST, membranes were scanned using the Odyssey Infrared Imaging System (LI-COR Biosciences, Lincoln, NE, USA). The following primary antibodies were used in this study at a dilution of 1:2000 unless otherwise noted: rat anti-HA antibody (Roche), rabbit anti-PDE6α (Pierce), rabbit anti-PDE6β (Pierce), rabbit anti-PDE6γ (Pierce), assembled PDE6 (ROS1) (generously provided by Drs Ted Wensel (Baylor College) and Rick Cote (University of New Hampshire), rabbit anti-Transducin-αt1 (Santa Cruz), mouse anti-cytochrome c oxidase subunit I (COX I) (MS404 MitoSciences), rabbit anti-Transducin-γt1 (Santa Cruz), mouse anti-GRK1 (Thermo Fisher), mouse anti-CNGA1 (UC Davis/NIH NeuroMab Facility), rabbit anti-RDS-c (Peripherin) (Gabriel Travis, University of California, Los Angeles, CA), mouse anti-1D4 (rhodopsin) (gift from Dr Ted Wensel, Baylor Collect of Medicine) and rabbit anti-ARL3 (1:1000) (this work). DAPI (1:1000) (4′,6-diamindino-2-phenylindole, Invitrogen) and propidium iodide (PI) (1:2000) (EMD Millipore, Billerica, MA, USA) were also used in indirect immunofluorescence.

Immunoprecipitation

Frozen retinas ($n = 4$) from ARL3-Q71L, ARL3-WT or transgenic negative animals were homogenized in 400 µl of 1× PBS containing protease inhibitors and 1 mM iodoacteamide using sonication (Fisher Scientific). The homogenized retinal extracts were centrifuged at 10 000*g* for 5 min and supernatant from this step was used for IP. The supernatant was then incubated for 2 h with washed anti-HA beads (Roche Biochemicals) at 4°C, followed by three rounds of washes with PBS + 0.1% TX-100, one wash with PBS and final elution with HA peptide at 37°C for 1 h. Proteins were then separated by 4–20% gradient SDS–PAGE and immunoblot was performed as described above.

Immunolocalization

For indirect immunofluorescence studies, enucleated eyes were immersed in 4% paraformaldehyde fixative for 5 min prior to removal of the anterior segments. Eyecups were fixed for an additional 1 h, washed in PBS for 20 min, incubated in 20% sucrose in PBS overnight at 4°C. Eyes were then incubated in 1:1 mixture of 20% sucrose in PBS:OCT (Cryo Optimal Cutting Temperature Compound, Sakura) for 1 h and flash-frozen in OCT. Cryosectioning was performed with a Leica CM1850 Cryostat, and serial retinal sections of 16 µm thickness were mounted on Superfrost Plus slides (Fisher Scientific). Retinal sections mounted on slides were washed with PBS and incubated for 1 h in blocking buffer (PBS with 5% goat sera, 0.5% TritonX-100, 0.05% sodium azide). Retinal sections were incubated with primary antibody at the dilutions indicated below for overnight at 4°C, followed by two 15 min washes with PBS + 0.1% TX-100, and one 10 min wash with PBS before incubation with secondary antibody at a 1:1000 dilution [DAPI nuclear stain 405, anti-Rat 568, anti-Rabbit 488 (or 568), anti-mouse 488 (or 568)] for 1 h. Slides were mounted with ProLong Gold (Life Technologies) and cover slipped. Confocal imaging was performed at the WVU Microscope Imaging Facility with a Zeiss LSM 510 laser scanning confocal on a LSM Axioimager upright microscope using excitation wavelengths of 405, 488 and 543 nm.

Hematoxylin&Eosin immunohistochemical analysis

Enucleated eyes were marked at the 12 o'clock position for reference with a red lipophilic dye and fixed in Excalibur Pathology Fixation Buffer at room temperature. These fixed whole eyes were then sent to Excalibur Pathology (Norman, OK) for paraffin embedding, sectioning at 2 µm and H&E staining. The stained sections were then imaged on a Zeiss light microscope. Analysis included measuring OS length from three different animals at three regions ventral and three regions dorsal to the optic nerve.

Ultrastructural analysis

Enucleated eyes were fixed (2% paraformaldehyde, 2.5% glutaraldehyde, 0.1 M cacodylate buffer, pH 7.5) for 30 min prior to dissection and removal of the anterior segment and lens, and extensively fixed for 48 h at room temperature. The fixed eyecup was dissected into 6–8 wedge-shaped pieces. Wedges were dehydrated in a graded ethanol series, and then embedded in Polybed 812 (PolySciences, Inc., Warrington, PA, USA). Semi-thin (1 µm) sections were collected onto glass slides, stained with toluidine blue and visualized using a Zeiss Axioimager 2 microscope equipped with EC Plan-Neofluar 40× (N.A. 0.75) and 100× (1.3 N.A.) objectives. Thin sections (ca. 80 nm) from selected wedges were collected onto nickel grids, stained with 2% uranyl acetate and lead citrate and imaged using an FEI Morgagni transmission electron microscope at 80 kV.

Supplementary Material

Supplementary Material is available at *HMG* online.

Acknowledgements

We thank Dr Peter Mathers and Ms Ingrid Weterrings of the West Virginia University (WVU) Transgenic Animal Core Facility for their help and services in generating our transgenic lines and Dr Karen Martin of the WVU Microscope Imaging Facility. We thank Drs Rick Cote, Ted Wensel and Gabriel Travis for sharing antibodies generated in their laboratories. We are indebted to the members of the Ramamurthy laboratory for their help and support throughout this study.

Conflict of Interest statement. None declared.

Funding

This work was supported by grants from the National Institutes of Health (EY017035 (to V.R.), EY019665 (to M.S.), R01EY013246 (to A.F.X.G.), RR017890 (to A.F.X.G.), West Virginia Lions, Lions Club International Fund and an Unrestricted Challenge Grant from Research to Prevent Blindness (RPB).

References

1. Sung, C.H. and Chuang, J.Z. (2010) The cell biology of vision. *J. Cell Biol.*, **190**, 953–963.
2. Pearring, J.N., Salinas, R.Y., Baker, S.A. and Arshavsky, V.Y. (2013) Protein sorting, targeting and trafficking in photoreceptor cells. *Prog. Retin. Eye Res.*, **36**, 24–51.
3. Schrick, J.J., Vogel, P., Abuin, A., Hampton, B. and Rice, D.S. (2006) ADP-ribosylation factor-like 3 is involved in kidney and photoreceptor development. *Am. J. Pathol.*, **168**, 1288–1298.
4. Gillingham, A.K. and Munro, S. (2007) The small G proteins of the Arf family and their regulators. *Annu. Rev. Cell Dev. Biol.*, **23**, 579–611.
5. Veltel, S., Gasper, R., Eisenacher, E. and Wittinghofer, A. (2008) The retinitis pigmentosa 2 gene product is a GTPase-activating protein for Arf-like 3. *Nat. Struct. Mol. Biol.*, **15**, 373–380.
6. Branham, K., Othman, M., Brumm, M., Karoukis, A.J., Atmaca-Sonmez, P., Yashar, B.M., Schwartz, S.B., Stover, N.B., Trzupek, K., Wheaton, D. *et al.* (2012) Mutations in RPGR and RP2 account for 15% of males with simplex retinal degenerative disease. *Investig. Ophthalmol. Vis. Sci.*, **53**, 8232–8237.
7. Zhang, H., Hanke-Gogokhia, C., Jiang, L., Li, X., Wang, P., Gerstner, C.D., Frederick, J.M., Yang, Z. and Baehr, W. (2015) Mistrafficking of prenylated proteins causes retinitis pigmentosa 2. *FASEB J.*, **29**, 932–942.
8. Bartolini, F., Bhamidipati, A., Thomas, S., Schwahn, U., Lewis, S.A. and Cowan, N.J. (2002) Functional overlap between retinitis pigmentosa 2 protein and the tubulin-specific chaperone cofactor C. *J. Biol. Chem.*, **277**, 14629–14634.
9. Ismail, S.A., Chen, Y.-X., Miertzschke, M., Vetter, I.R., Koerner, C. and Wittinghofer, A. (2012) Structural basis for Arl3-specific release of myristoylated ciliary cargo from UNC119. *EMBO J.*, **31**, 4085–4094.
10. Wätzlich, D., Vetter, I., Gotthardt, K., Miertzschke, M., Chen, Y.-X., Wittinghofer, A. and Ismail, S. (2013) The interplay between RPGR, PDEδ and Arl2/3 regulate the ciliary targeting of farnesylated cargo. *EMBO Rep.*, **14**, 465–472.
11. Ismail, S.A., Chen, Y.-X., Rusinova, A., Chandra, A., Bierbaum, M., Gremer, L., Triola, G., Waldmann, H., Bastiaens, P.I.H. and Wittinghofer, A. (2011) Arl2-GTP and Arl3-GTP regulate a GDI-like transport system for farnesylated cargo. *Nat. Chem. Biol.*, **7**, 942–949.
12. Zhang, H., Li, S., Doan, T., Rieke, F., Detwiler, P.B., Frederick, J.M. and Baehr, W. (2007) Deletion of PrBP/delta impedes transport of GRK1 and PDE6 catalytic subunits to photoreceptor outer segments. *Proc. Natl Acad. Sci. USA*, **104**, 8857–8862.

13. Li, L., Khan, N., Hurd, T., Ghosh, A.K., Cheng, C., Molday, R., Heckenlively, J.R., Swaroop, A. and Khanna, H. (2013) Ablation of the X-linked retinitis pigmentosa 2 (Rp2) gene in mice results in opsin mislocalization and photoreceptor degeneration. *Investig. Ophthalmol. Vis. Sci.*, **54**, 4503–4511.
14. Liu, F., Chen, J., Yu, S., Raghupathy, R.K., Liu, X., Qin, Y., Li, C., Huang, M., Liao, S., Wang, J. *et al.* (2015) Knockout of RP2 decreases GRK1 and rod transducin subunits and leads to photoreceptor degeneration in zebrafish. *Hum. Mol. Genet.* **24**, 4648–4659.
15. Song, H., Bush, R.A., Vijayasarathy, C., Fariss, R.N., Kjellstrom, S. and Sieving, P.A. (2014) Transgenic expression of constitutively active RAC1 disrupts mouse rod morphogenesis. *Invest. Ophthalmol. Vis. Sci.*, **55**, 2659–2668.
16. Grayson, C., Bartolini, F., Chapple, J.P., Willison, K.R., Bhamidipati, A., Lewis, S.A., Luthert, P.J., Hardcastle, A.J., Cowan, N.J. and Cheetham, M.E. (2002) Localization in the human retina of the X-linked retinitis pigmentosa protein RP2, its homologue cofactor C and the RP2 interacting protein Arl3. *Hum. Mol. Genet.*, **11**, 3065–3074.
17. Song, H. and Sokolov, M. (2009) Analysis of protein expression and compartmentalization in retinal neurons using serial tangential sectioning of the retina. *J. Proteome Res.*, **8**, 346–351.
18. Belcastro, M., Song, H., Sinha, S., Song, C., Mathers, P.H. and Sokolov, M. (2012) Phosphorylation of phosducin accelerates rod recovery from transducin translocation. *Invest. Ophthalmol. Vis. Sci.*, **53**, 3084–3091.
19. Lyubarsky, A.L., Chen, C., Simon, M.I. and Pugh, E.N. (2000) Mice lacking G-protein receptor kinase 1 have profoundly slowed recovery of cone-driven retinal responses. *J. Neurosci.*, **20**, 2209–2217.
20. Cideciyan, A.V., Zhao, X., Nielsen, L., Khani, S.C., Jacobson, S.G. and Palczewski, K. (1998) Null mutation in the rhodopsin kinase gene slows recovery kinetics of rod and cone phototransduction in man. *Proc. Natl Acad. Sci. USA*, **95**, 328–333.
21. Chen, C.K., Burns, M.E., Spencer, M., Niemi, G.A., Chen, J., Hurley, J.B., Baylor, D.A. and Simon, M.I. (1999) Abnormal photoresponses and light-induced apoptosis in rods lacking rhodopsin kinase. *Proc. Natl Acad. Sci. USA*, **96**, 3718–3722.
22. Kolandaivelu, S., Singh, R.K. and Ramamurthy, V. (2014) AIPL1, a protein linked to blindness, is essential for the stability of enzymes mediating cGMP metabolism in cone photoreceptor cells. *Hum. Mol. Genet.*, **23**, 1002–1012.
23. Wright, K.J., Baye, L.M., Olivier-Mason, A., Mukhopadhyay, S., Sang, L., Kwong, M., Wang, W., Pretorius, P.R., Sheffield, V.C., Sengupta, P. *et al.* (2011) An ARL3-UNC119-RP2 GTPase cycle targets myristoylated NPHP3 to the primary cilium. *Genes Dev.*, **25**, 2347–2360.
24. Baehr, W. (2014) Membrane protein transport in photoreceptors: the function of PDE. *Invest. Ophthalmol. Vis. Sci.*, **55**, 8653–8666.
25. Kizilyaprak, C., Spehner, D., Devys, D. and Schultz, P. (2010) *In vivo* chromatin organization of mouse rod photoreceptors correlates with histone modifications. *PLoS One*, **5**, e11039.
26. Carter-Dawson, L.D. and LaVail, M.M. (1979) Rods and cones in the mouse retina. I. Structural analysis using light and electron microscopy. *J. Comp. Neurol.*, **188**, 245–262.
27. Jin, M., Yamada, M., Arai, Y., Nagai, T. and Hirotsune, S. (2014) Arl3 and LC8 regulate dissociation of dynactin from dynein. *Nat. Commun.*, **5**, 5295.
28. Kim, H., Xu, H., Yao, Q., Li, W., Huang, Q., Outeda, P., Cebotaru, V., Chiaravalli, M., Boletta, A., Piontek, K. *et al.* (2014) Ciliary membrane proteins traffic through the Golgi via a Rabep1/GGA1/Arl3-dependent mechanism. *Nat. Commun.*, **5**, 5482.
29. Kahn, R.A., Volpicelli-Daley, L., Bowzard, B., Shrivastava-Ranjan, P., Li, Y., Zhou, C. and Cunningham, L. (2005) Arf family GTPases: roles in membrane traffic and microtubule dynamics. *Biochem. Soc. Trans.*, **33**, 1269–1272.
30. Zhou, C., Cunningham, L., Marcus, A., Li, Y. and Kahn, R.A. (2006) Arl2 and Arl3 regulate different microtubule-dependent processes. *Mol. Biol. Cell*, **17**, 2476–2487.
31. Zhang, Q., Hu, J. and Ling, K. (2013) Molecular views of Arf-like small GTPases in cilia and ciliopathies. *Exp. Cell Res.*, **319**, 2316–2322.
32. Evans, R.J., Schwarz, N., Nagel-Wolfrum, K., Wolfrum, U., Hardcastle, A.J. and Cheetham, M.E. (2010) The retinitis pigmentosa protein RP2 links pericentriolar vesicle transport between the Golgi and the primary cilium. *Hum. Mol. Genet.*, **19**, 1358–1367.
33. Yu, J., Lei, K., Zhou, M., Craft, C.M., Xu, G., Xu, T., Zhuang, Y., Xu, R. and Han, M. (2011) KASH protein Syne-2/Nesprin-2 and SUN proteins SUN1/2 mediate nuclear migration during mammalian retinal development. *Hum. Mol. Genet.*, **20**, 1061–1073.
34. Adam, S.A., Butin-Israeli, V., Cleland, M.M., Shimi, T. and Goldman, R.D. (2013) Disruption of lamin B1 and lamin B2 processing and localization by farnesyltransferase inhibitors. *Nucleus*, **4**, 142–150.
35. Coffinier, C., Jung, H.-J., Nobumori, C., Chang, S., Tu, Y., Barnes, R.H., Yoshinaga, Y., de Jong, P.J., Vergnes, L., Reue, K. *et al.* (2011) Deficiencies in lamin B1 and lamin B2 cause neurodevelopmental defects and distinct nuclear shape abnormalities in neurons. *Mol. Biol. Cell*, **22**, 4683–4693.
36. Humbert, M.C., Weihbrecht, K., Searby, C.C., Li, Y., Pope, R.M., Sheffield, V.C. and Seo, S. (2012) ARL13B, PDE6D, and CEP164 form a functional network for INPP5E ciliary targeting. *Proc. Natl Acad. Sci. USA*, **109**, 19691–19696.
37. Cavenagh, M., Breiner, M., Schürmann, A., Rosenwald, A., Terui, T., Zhang, C., Randazzo, P., Adams, M., Joost, H. and Kahn, R. (1994) ADP-ribosylation factor (ARF)-like 3, a new member of the ARF family of GTP-binding proteins cloned from human and rat tissues. *J. Biol. Chem.*, **269**, 18937–18942.
38. Wynshaw-Boris, A. and Gambello, M.J. (2001) LIS1 and dynein motor function in neuronal migration and development. *Genes Dev.*, **15**, 639–651.
39. Kähler, A.K., Djurovic, S., Kulle, B., Jönsson, E.G., Agartz, I., Hall, H., Opjordsmoen, S., Jakobsen, K.D., Hansen, T., Melle, I. *et al.* (2008) Association analysis of schizophrenia on 18 genes involved in neuronal migration: MDGA1 as a new susceptibility gene. *Am. J. Med. Genet. B. Neuropsychiatr. Genet.*, **147B**, 1089–1100.
40. Deutsch, S.I., Burket, J.A. and Katz, E. (2010) Does subtle disturbance of neuronal migration contribute to schizophrenia and other neurodevelopmental disorders? Potential genetic mechanisms with possible treatment implications. *Eur. Neuropsychopharmacol.*, **20**, 281–287.
41. Wegiel, J., Kuchna, I., Nowicki, K., Imaki, H., Wegiel, J., Marchi, E., Ma, S.Y., Chauhan, A., Chauhan, V., Bobrowicz, T.W. *et al.* (2010) The neuropathology of autism: defects of neurogenesis and neuronal migration, and dysplastic changes. *Acta Neuropathol.*, **119**, 755–770.
42. Chandra, A., Grecco, H.E., Pisupati, V., Perera, D., Cassidy, L., Skoulidis, F., Ismail, S.A., Hedberg, C., Hanzal-Bayer, M., Venkitaraman, A.R. *et al.* (2012) The GDI-like solubilizing factor

PDEδ sustains the spatial organization and signalling of Ras family proteins. *Nat. Cell Biol.*, **14**, 329–329.
43. Apolloni, A., Prior, I.A., Lindsay, M., Parton, R.G. and Hancock, J.F. (2000) H-ras but not K-ras traffics to the plasma membrane through the exocytic pathway. *Mol. Cell. Biol.*, **20**, 2475–2487.
44. Gotthardt, K., Lokaj, M., Koerner, C., Falk, N., Gießl, A. and Wittinghofer, A. (2015) A G-protein activation cascade from Arl13B to Arl3 and implications for ciliary targeting of lipidated proteins. *Elife*, **4**, e11859.
45. Datta, P., Allamargot, C., Hudson, J.S., Andersen, E.K., Bhattarai, S., Drack, A.V., Sheffield, V.C. and Seo, S. (2015) Accumulation of non-outer segment proteins in the outer segment underlies photoreceptor degeneration in Bardet–Biedl syndrome. *Proc. Natl Acad. Sci.*, **112**, E4400–E4409.
46. Giménez, E. and Montoliu, L. (2001) A simple polymerase chain reaction assay for genotyping the retinal degeneration mutation (Pdeb(rd1)) in FVB/N-derived transgenic mice. *Lab. Anim.*, **35**, 153–156.